The pressure–hole problem

By C. DUCRUET† AND A. DYMENT‡

I.M.F.L., 5 bd Painlevé, 59000 Lille, France

The static pressure–hole problem is investigated both theoretically and experimentally. The influence of all significant dimensionless parameters is brought to light. These parameters represent the effects of the boundary layer, of the velocity gradient and of the wall curvature. A partial linearization makes it possible to propose a formula of correction containing three influence functions which cannot be determined by the theory. A limited number of experiments on appropriate models leads to the determination of these functions in case of practical requirements. So, a method of correction is obtained, but only in incompressible flow. The previous formula has been verified in two complex flows. The importance of the correction on the pressure drag of a slender body is brought to light and the difficulties in the application on the method are emphasized.

1. Introduction

The wall pressure in a flow is usually measured by drilling a hole and connecting it to a manometer. The consequence of the local perturbation generated by a hole of diameter d is that the measured pressure p_d is somewhat different from the true pressure p_0 corresponding to $d = 0$.

This problem has already been studied on several occasions, mainly in turbulent pipe flow (Shaw 1960; Ray 1956; Livesey, Jackson & Southern 1962; Franklin & Wallace 1970; Myadzu 1936; L. C. Squire 1983 private communication). (For an extensive bibliography see Barat (1973) and Chue (1979).) Some experiments have also been made in high-speed flow (Flack 1978; Moulden *et al.* 1977; Morrisson, Sheppard & Williams 1966; Pugh, Peto & Ward 1970; Rainbird 1967; Rayle 1949). The results thus obtained are incomplete; furthermore they do not entirely coincide with each other, so that the problem still remains unsolved.

One result which seems unquestionable is the fact that the error $p_d - p_0$ is an increasing function of d. As it is very difficult to drill holes smaller than 0.2 mm in diameter, and as, on the other hand, wind-tunnel models are not large, the error must often be taken into account. This is especially true when pressure measurements are used to determine a small quantity such as, for instance, the drag coefficient of a slender body.

The aim of this paper is to provide a universal method of correction (Ducruet 1983 *a, b*; Ducruet & Dyment 1981).

Our work is restricted to steady incompressible flows. First we collect the dimensionless parameters which are significant for the problem. An analysis of the phenomenon and some experimental investigations show that the influence of the hole Reynolds number can be eliminated. This simplification yields the result that, for

---

† Permanent address: E.N.S.I., 59326 Valenciennes Cedex, France.
‡ Permanent address: Université de Lille I, 59655 Villeneuve d'Ascq Cedex, France.

holes of a given depth-to-diameter ratio h/d, only three characteristic parameters are significant. Next, a partial linearization enables us to separate the effects of both velocity gradient and wall curvature.

The previous theoretical approach leads to a formula of correction in which there appear to be three functions of the boundary-layer parameter and of the depth-to-diameter ratio. These functions must be determined experimentally.

The effect of the boundary layer alone has been investigated in experiments on a flat plate, both in laminar and turbulent regimes.

The influence of the velocity gradient has been estimated on various wedges in order to cancel the curvature effects.

The influence of the wall curvature has been studied in experiments with coaxial rotating cylinders, since the velocity gradient is zero in that flow.

In all our tests two values of h/d have been considered.

As the pressure error to be detected is very small, it cannot be evaluated in any other way than by simultaneous and direct differential measurements made between holes of different diameters located on the same generatrix of the model. The exact pressure is obtained by extrapolation to $d = 0$. This process is quite accurate because the extrapolated result must be the same for any value of h/d.

The method we are putting forward has been applied at first to the flow around a cylinder. It has been verified that the superposition of the three elementary errors contained in the formula provides a result which is very close to the actual error, directly obtained by extrapolation to $d = 0$ of measurements made on the cylinder.

Another verification has been carried out on the flow around an airfoil. Measurements made for two sets of orifices of different diameters lead to the same value of the corrected pressure. The drag obtained by integrating the pressure thus measured is considerably different from the actual drag.

2. Dimensional analysis

Let us suppose that the flow is two-dimensional and that the rear of the orifice is large compared with d. The properties of the fluid in the vicinity of the orifice can be produced by a number of different flows: this means that we have to consider the problem from a local point of view.

The fluid is characterized by its density ρ and its kinematic viscosity ν.

The wall can be locally represented by its osculating circle of diameter D. Let $Oxyz$ be the system of axes shown on figure 1. The no-slip condition holds for $x^2 + y^2 = \frac{1}{4}d^2$, $-h \leqslant z \leqslant 0$, and for $x^2 + z^2 + Dz = 0$.

As the disturbances created by the hole are small, the boundary layer remains almost the same as when $d = 0$. Let u_e be the external velocity and u the velocity inside the boundary layer. The velocity profile can be expressed in terms of z/θ and $\theta^2 u_{ex}/\nu$, θ being the momentum thickness and u_{ex} the local velocity gradient (Schlichting 1979).

It follows from the previous considerations that the parameters which go into the problem are ρ, ν, d, h, D, θ, u_e and u_{ex}. The pressure p_e outside the boundary layer does not interfere because the fluid is incompressible. When applying the Vaschy–Buckingham theorem one obtains (Ducruet 1983a; Ducruet & Dyment 1981):

$$\frac{p_d - p_0}{\frac{1}{2}\rho u_e^2} = \psi\left(\frac{u_e d}{\nu}, \frac{u_{ex} d}{u_e}, \frac{d}{D}, \frac{d}{\theta}, \frac{h}{d}\right). \tag{1}$$
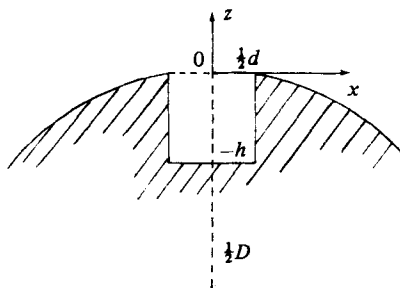
FIGURE 1. A schematic representation of a cavity.

When the flow is three-dimensional D represents the diameter of the osculating sphere. It is usually admitted that the parameters which characterize the transverse velocity along Oy in the boundary layer are the same as those concerning u/u_e, which is calculated as in a two-dimensional flow (Eichelbrenner 1958). Consequently (1) still holds for three-dimensional flow, at least as a first approximation.

3. Effect of the Reynolds number

Let us consider similar orifices (h/d constant). For d very close to zero the flow in the vicinity of the orifice may be regarded as creeping. Therefore ρ disappears from the set of parameters and (1) is replaced by

$$(p_d - p_0)\frac{d}{\rho \nu u_e} = \chi\left(\frac{u_{ex}d}{u_e}, \frac{d}{D}, \frac{d}{\theta}\right) \tag{2}$$

or

$$\frac{p_d - p_0}{\frac{1}{2}\rho u_e^2} = \frac{2}{R_e}\chi, \tag{3}$$

with $R_e = u_e d/\nu$.

As d is small the function χ can be expanded. For $d = 0$, χ and its first derivatives must vanish in order to obtain $p_d = p_0$. As a result the expansion begins with terms proportional to d^2, so that $p_d - p_0$ is proportional to $\rho\nu d$.

Consider now larger values of R_e. Above a certain value $\tilde{R}_e$ the shear layer that separates the fluid inside the orifice from that outside becomes unstable and produces a mixing layer. Thus, for $R_e > \tilde{R}_e$ the phenomenon is independent of the viscosity, and consequently R_e must disappear from (1).

A rough estimate of $\tilde{R}_e$ has been obtained by visualization in a free-surface water channel (Ducruet 1983a). The orifice was represented by a vertical slot containing coloured water. The freestream velocity being gradually increased, the value $\tilde{R}_e$ is reached as soon as the external flow becomes coloured. That occurs for $\tilde{R}_e \approx 40$. In similar experiments carried out with cylindrical holes, the value obtained for $\tilde{R}_e$ was about 250 (Squire 1983 private communication). Consequently the range of values of d corresponding to $R_e < \tilde{R}_e$ is very narrow. For instance, with ambient air, $u_e = 30$ m/s and $\tilde{R}_e = 250$, we get $d \approx 10^{-1}$ mm!

An attempt was made to ensure that the hole Reynolds number has no influence. It is rather difficult to change each dimensionless parameter separately, but we succeeded in doing it with the rotating cylinders described in §8 below. We found that, within the range 840–3685, $u_e d/\nu$ has no influence on the dimensionless pressure error.

The previous result shows that, when we leave R_e out, our analysis is still valid, but for a very minute domain close to $d = 0$. Hence (1) can be written

$$\frac{p_d - p_0}{\frac{1}{2}\rho u_e^2} = \phi\left(\frac{u_{ex}d}{u_e}, \frac{d}{D}, \frac{d}{\theta}\right). \tag{4}$$

It must be noticed that, for orifices located in the vicinity of a stagnation point, where the velocity is low, the condition $R_e > \tilde{R}_e$ may not be fulfilled.

Precisely, at a stagnation point the representation (1) is not valid because $u_e = 0$. It is replaced by

$$\frac{p_d - p_0}{\rho\nu u_{ex}} = \Omega\left(\frac{u_{ex}d^2}{\nu}, \frac{d}{D}, \frac{d}{\theta}\right).$$

But, as $\theta(u_{ex}/\nu)^{\frac{1}{2}}$ is constant (Schlichting 1979), we obtain

$$\frac{p_d - p_0}{\rho\nu u_{ex}} = \Lambda\left(\frac{d}{D}, \frac{d}{\theta}\right). \tag{5}$$

If we consider the flow around the osculating cylinder we have (Schlichting 1979) $u_{ex} = 4u_\infty/D$, where u_∞ is the freestream velocity (a similar relation holds in three-dimensional flow for the osculating sphere). This means that (5) can also be written

$$\frac{p_d - p_0}{\frac{1}{2}\rho u_\infty^2} = \Gamma\left(\frac{d}{D}, \frac{d}{\theta}\right). \tag{6}$$

Let us now consider an orifice located in the separated domain behind a thick body. Such a domain depends almost entirely on the transverse size H of the body. Moreover, we are supposing that the error is independent of the position of the orifice except very close to separation or rear stagnation points. Therefore the error is a function of ρ, ν, u_∞, H and d. As there is a mixing layer at the entrance of the orifice, ν disappears and we obtain (Ducruet 1983a)

$$\frac{p_d - p_0}{\frac{1}{2}\rho u_\infty^2} = \Sigma\left(\frac{d}{H}\right). \tag{7}$$

4. Linearization

Let us return to the general case. As the dimensionless parameters $u_{ex}d/u_e$ and d/D are always small, we can do a partial linearization of (4) and write (Ducruet 1983a; Ducruet & Dyment 1981)

$$\frac{p_d - p_0}{\frac{1}{2}\rho u_e^2} = F + G_v\frac{u_{ex}d}{u_e} + G_c\frac{d}{D}. \tag{8}$$

The influence functions F, G_v and G_c depend on d/θ, on h/d and on the nature of the boundary layer, whether laminar or turbulent.

For $d \ll \theta$ a completely linearized formula can be written:

$$\frac{p_d - p_0}{\frac{1}{2}\rho u_e^2} = I_\theta\frac{d}{\theta} + I_v\frac{u_{ex}d}{u_e} + I_c\frac{d}{D}. \tag{9}$$

On the other hand, for $d \gg \theta$, the function F can be restricted to its asymptotic value, say F_1. Now denoting the values of G_v and G_c by J_v and J_c, we obtain

$$\frac{p_d - p_0}{\frac{1}{2}\rho u_e^2} = F_1 + J_v\frac{u_{ex}d}{u_e} + J_c\frac{d}{D}. \tag{10}$$

Owing to the linearization the influences of $u_{ex}d/u_e$ and d/D are independent. The influence of the boundary layer is independent too, but only in the extreme cases $d \ll \theta$ and $d \gg \theta$. The coefficients I_θ, I_v, I_c, F_1, J_v and J_c are functions of h/d, but only I_θ and F_1 depend on the nature of the boundary layer.

All the previous results may be extended to high-speed flow (Ducruet 1983 a). In this case ρ is replaced by ρ_e and p_e must be taken into account. The corresponding dimensionless parameter is the local Mach number M_e, so that now the influence functions also depend on M_e.

5. Experimental methods

The functions F, G_v and G_c can only be determined experimentally.

The influences of the boundary layer and of the velocity gradient have been investigated in a continuous-running closed-circuit wind tunnel. The test section is 450×450 mm² in size. The upstream velocity u_∞ was close to 25 m/s and the intensity of the turbulence was about 0.37 %.

Measurements give access to the pressure coefficient $K_d = (p_d - p_\infty)/\frac{1}{2}\rho u_\infty^2$, p_∞ being the undisturbed flow pressure. The Bernoulli law enables us to write

$$\frac{p_e - p_\infty}{\frac{1}{2}\rho u_e^2} = \frac{u_\infty^2}{u_e^2} - 1.$$

On the other hand, $(p_e - p_0)/\frac{1}{2}\rho u_e^2$ is proportional to θ/D (Schlichting 1979) and even to θ^2 when the wall is flat. Thus this quantity is negligible and we obtain

$$\frac{p_d - p_0}{\frac{1}{2}\rho u_e^2} = (K_d - 1)\frac{u_\infty^2}{u_e^2} + 1. \tag{11}$$

For $d = 0$. $K_d = K_0$, so that finally

$$\frac{p_d - p_0}{\frac{1}{2}\rho u_e^2} = \frac{K_d - K_0}{1 - K_0}. \tag{12}$$

Pressure measurements have been achieved with 'Debro Miniscope' micromanometers. Their main characteristic is that the measurement is made through a sighting telescope, magnifying ten times and which can be adjusted with a micrometric screw. The reading is made directly, without any parallax error. The accuracy of these instruments is estimated at about 2×10^{-2} mm of water. The result is that only differences between measured values of K_d larger than 10^{-3} have some significance. The high response time of these instruments constitutes a major drawback.

The influence of the wall curvature has been studied in flows between coaxial cylinders (Ducruet 1983 a, b). The inner cylinder of diameter D was fixed and the outer cylinder was rotating.

All the models are equipped with holes of depth-to-diameter ratio equal to 3 and 1. The holes are perpendicular to the wall. The cavity behind the pressure hole is cylindrical and of diameter d_c much larger than d in order to eliminate the influence of d_c/d. The quality of the boring was verified by a careful examination with a microscope magnifying 50 times and yielding a measurement of d with an accuracy of 10^{-2} mm. The holes were drilled in cylindrical plugs, which were afterwards inserted into the model. That way a defective hole could easily be replaced. The smallest diameter which we tested was 0.2 mm.

The pressure error to be detected is very small: it must be estimated by a direct
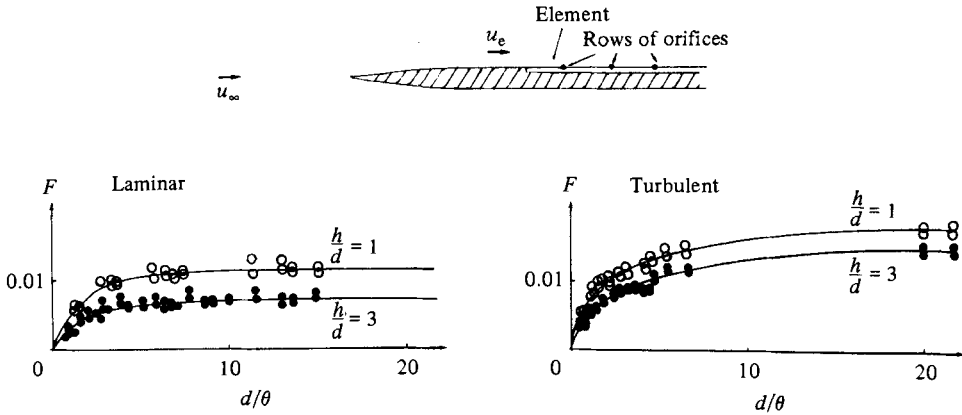
FIGURE 2. Influence of the boundary layer.
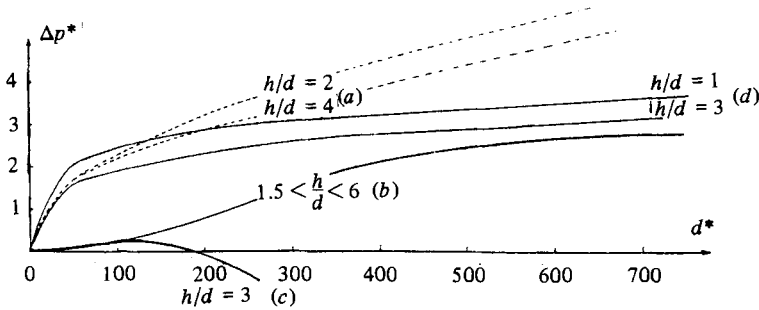
FIGURE 3. Influence of the turbulent layer: (a) Ray (1956); (b) Shaw (1960); (c) Livesey *et al.* (1962); (d) present results.

differential measurement. Consequently, models must be two-dimensional, and we can only take into consideration simultaneous measurements between orifices located on the same generatrix. This requires that the flow be rigorously the same spanwise.

All models are equipped with interchangeable elements corresponding to a given value of h/d and made up of rows of orifices of different diameter, located along generatrices of the model. Obviously, great care must be taken in positioning the orifices exactly. The distance between neighbouring orifices was chosen sufficiently large to avoid any mutual influence. This distance has been roughly evaluated by preliminary experiments (Ducruet 1983a).

The true coefficient K_0 is obtained by extrapolation to $d = 0$ of the plots of K_d versus d. This extrapolation has a good accuracy because we have at least two curves corresponding to different values of h/d: as K_0 is independent of h/d, all curves must provide the same extrapolated value. A slight difficulty may appear in the vicinity of $d = 0$. According to the reasoning in §3, for $d < \tilde{d}$ the dimensionless error $(p_d - p_0)/\frac{1}{2}\rho u_e^2$ is represented by a set of curves with $u_e d/\nu$ as a parameter; but for $d > \tilde{d}$ there is only one curve, because the error no longer depends on $u_e d/\nu$. As the first point is obtained for $d \approx 0.2$ mm, it is obvious that the range $d < \tilde{d}$ cannot be reached in experiments. But in fact the resulting error is smaller than the error due to the pressure measurement.

6. Influence of the boundary layer

The function F, which represents the effects of the boundary layer alone, has been determined by means of experiments in an external flow without velocity gradient and curvature. Consequently the chosen model was a flat plate at zero angle of attack. The model is 500 mm long and 18 mm thick. The leading edge has such a form that the velocity gradient is positive and vanishes smoothly after a distance of about 100 mm. A housing, 200 mm long, is hollowed in the central part in order to receive an element equipped with 5 rows of orifices. Five elements have been constructed in order to obtain a large number of values of d/θ. For tests with a turbulent boundary layer, artificial transition was instigated near the leading edge.

In each case the boundary-layer velocity profile was obtained with the help of a small total-pressure probe. It was verified that the velocity profiles coincide with the classical laminar and turbulent curves.

The values of K_d derived from measurements at every row of orifices give the exact value K_0 by extrapolation. Next K_0 is used to calculate F with the help of (12). The final results are given in figure 2. We can see that F is an increasing function of d/θ: the error is more important when the boundary layer is turbulent and moreover it is larger for $h/d = 1$ than for $h/d = 3$. The asymptote F_1 is reached for $d \approx 8\theta$ in the laminar case and $d \approx 15\theta$ in the turbulent one: these values roughly correspond to the boundary-layer thickness. F_1 is determined accurately, as opposed to the coefficient I_θ, which is equal to the slope at the origin.

For comparison with results obtained in the past for turbulent flow (Shaw 1960; Ray 1956; Livesey *et al.* 1962) F and d/θ must be changed into $\Delta p^* = (p_d - p_0)/\tau$ and $d^* = (d/\nu)(\tau/\rho)^{\frac{1}{2}}$, where τ is the wall shear stress. The transformation has been performed by using the $\frac{1}{7}$-power law for the velocity profile (Schlichting 1979). The comparison is shown on figure 3. Our results are close to those of Ray (1956) for small values of d and to those of Shaw (1960) for large values; but they are in complete disagreement with those of Livesey *et al.* (1962).

7. Influence of the velocity gradient

The function G_v must be determined in experiments on flat walls in order to cancel the curvature effects. Of course, the boundary-layer influence cannot be avoided, and measurements enable us to compute $F + G_v u_{ex} d/u_e$. As F is already known, G_v can easily be deduced.

Two types of models have been tested in order to cover the whole range of variation of d/θ. For $d \gg \theta$ we have used wedges of total angle $\phi = 30°$, $60°$ and $90°$. Let x be the distance from the apex. The theoretical expression for u_e should be Cx^n, with C constant and $\phi = 2\pi n/(n+1)$. Since the model is finite and because the flow is restricted by the walls, the actual exponent n' given by pressure measurements is somewhat different from n. We can define a fictitious angle ϕ' such that $\phi' = 2\pi n'/(n'+1)$. We then have $u_{ex}/u_e = n'/x$, and θ is obtained by the well-known Falkner–Skan solution (Schlichting 1979).

The model can receive two interchangeable elements containing two rows of orifices located at the stations $x = 10$ mm and 24 mm.

Some results concerning K_d are shown on figure 4 as an example. These should serve to demonstrate the accuracy of the extrapolation. From the extrapolated value K_0 we can derive u_e/u_∞ by $(K_0 - 1) u_\infty^2/u_e^2 + 1 = 0$ resulting from (11). Then u_e, n', ϕ', u_{ex}/u_e and θ are obtained easily. Finally (12) is used to obtain the error, which is
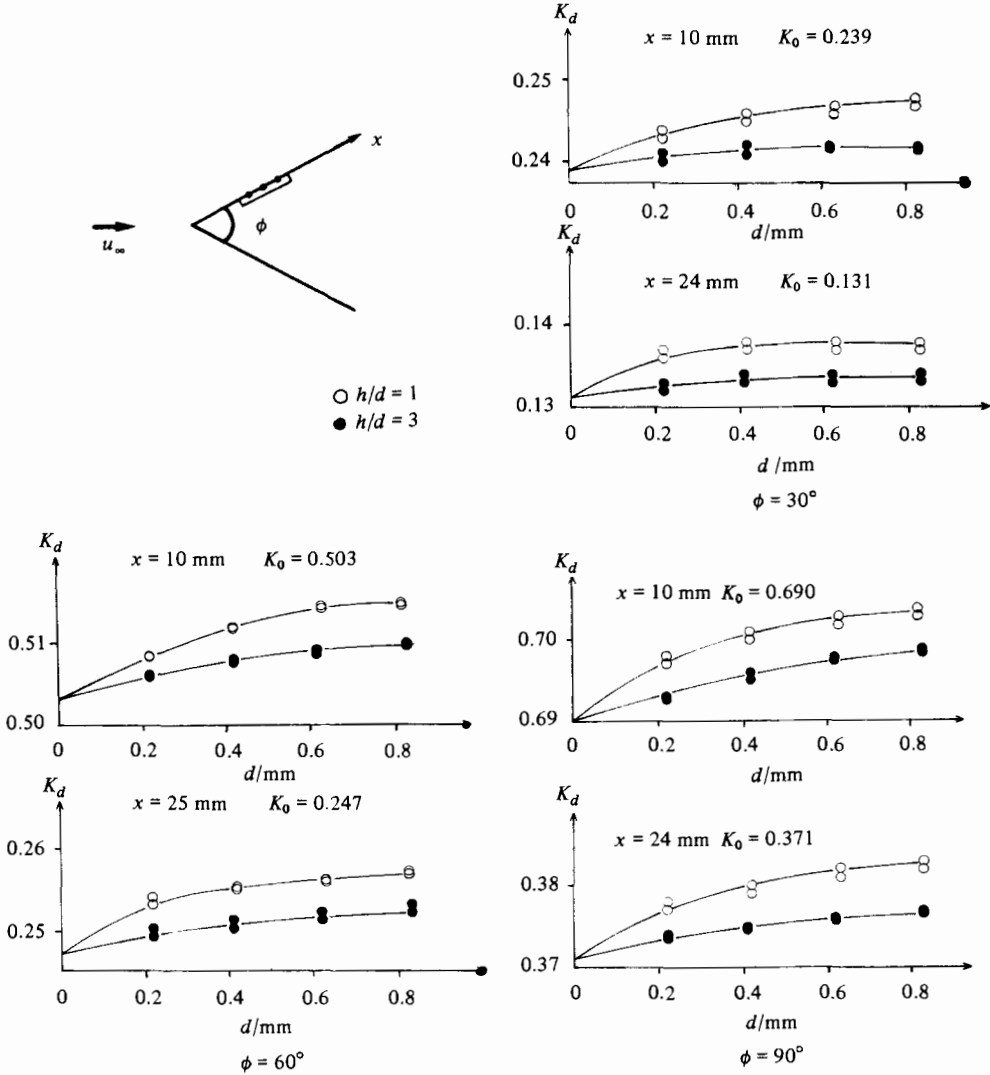
FIGURE 4. Experiments on wedges in laminar flow.

shown versus $u_{ex}d/u_e$ on figure 5. Only the curve corresponding to $d \gg \theta$ can be drawn accurately: it is a straight line with slope J_v intersecting the $d = 0$ axis at F_1.

In the model intended for experiments for $d \sim \theta$ and $d \ll \theta$, two wedges with slopes $45°$ and $60°$ were constructed. They were preceded by a flat plate long enough to thicken the boundary layer. The joint between the plate and the wedge was made round to avoid separation. Four elements equipped with two rows of orifices were used. A fifth one, equipped with very small total probes, was used exclusively for exploring the turbulent boundary layer at the stations where orifices are located.

As previously, K_0 is obtained by extrapolation from the measured values of K_d; then the error is deduced from (12). The results are shown versus $u_{ex}d/u_e$ for constant d/θ on figure 6. The ordinate at origin is the turbulent value of F previously obtained. We can see that, at least for values of d/θ for which more than two points exist, the
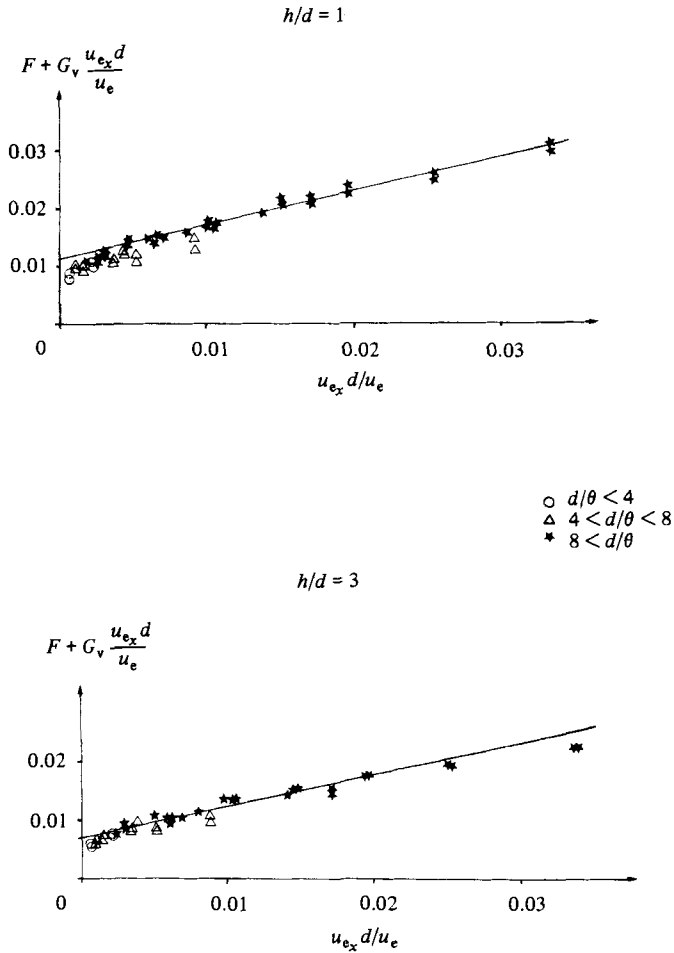
FIGURE 5. Determination of G_v in laminar flow.

linear formula is appropriate. The slope of the drawn lines provides G_v in turbulent flow. On the same figure we have also plotted the line of slope J_v but with the value of F_1 corresponding to the turbulent regime.

As $d/\theta = 0$ cannot be experimentally achieved, the coefficient I_v must be determined as the limiting value of G_v when d/θ tends towards zero. It seems that this asymptotic value is almost reached for $d/\theta \approx 0.2$. Of course, I_v is not accurately known. But, from a practical point of view this is not very important because, when put into practice, the value I_v is hardly ever needed: on a model in a wind tunnel, values such as $d \ll \theta$ are found far from the leading edge, where $u_{ex}d/u_e$ is very small, so that the correction only comes from the boundary-layer effect.

To summarize, we have obtained J_v and G_v for $d/\theta > 2$ in laminar flow, and I_v and G_v for $d/\theta < 2$ in turbulent flow. These cases are the most common ones encountered on an airfoil. All our results are gathered on figure 7. As J_v and I_v are the same in both laminar and turbulent flows, it appears on the whole that G_v depends very little on the nature of the boundary layer (Ducruet 1983a; Ducruet & Dyment 1981).
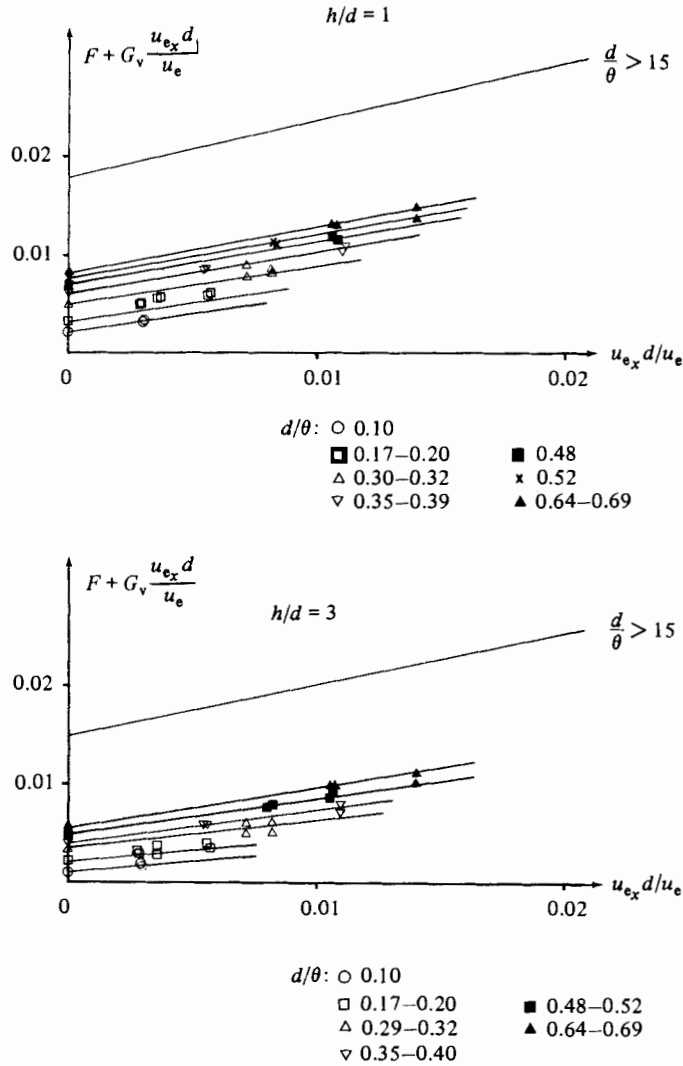
FIGURE 6. Determination of G_v in turbulent flow.
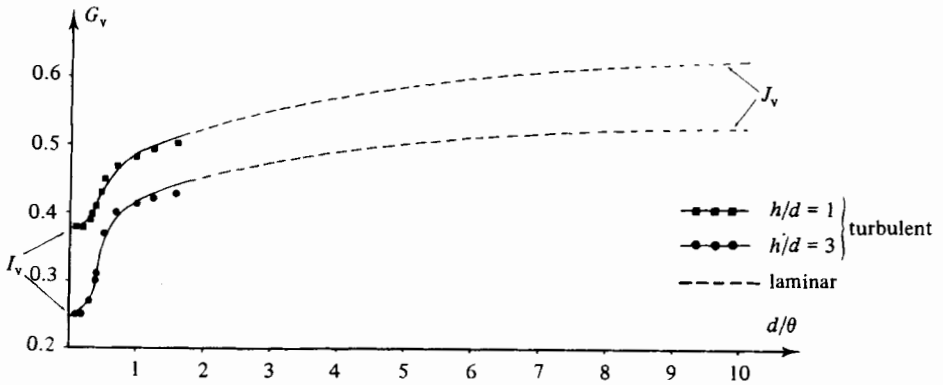
FIGURE 7. Influence of the velocity gradient.
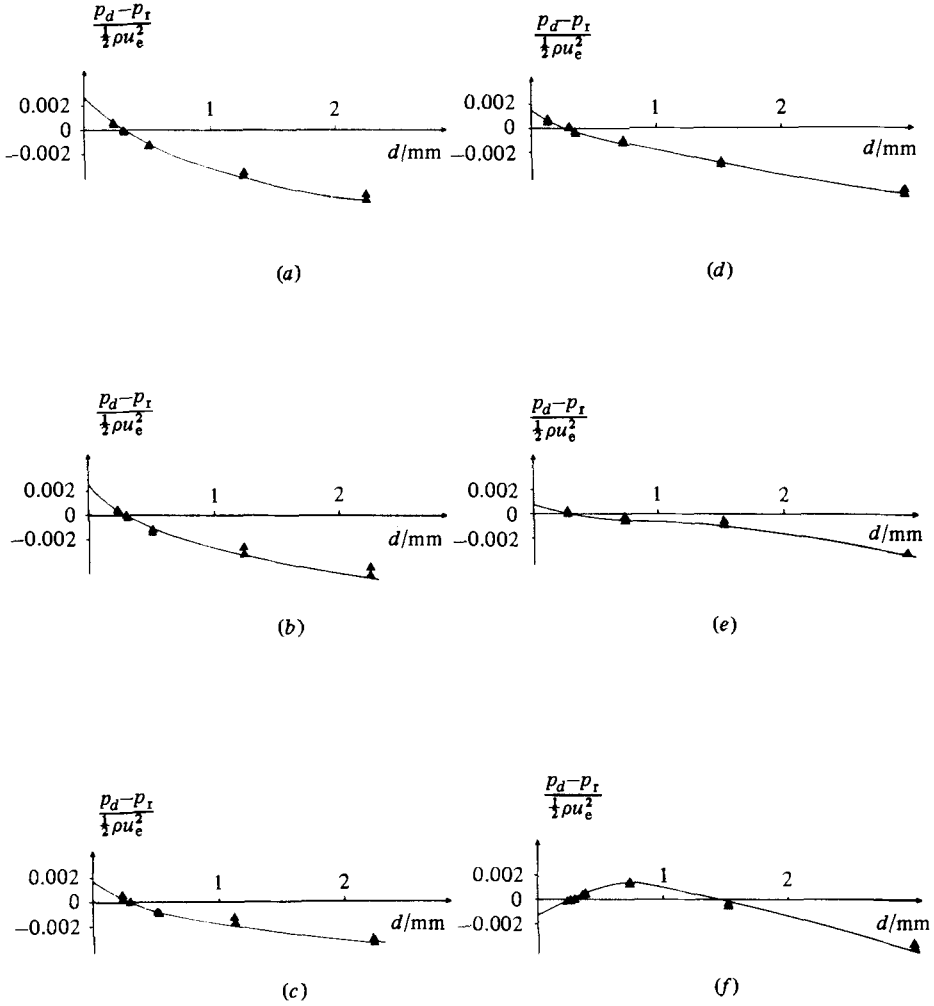
FIGURE 8. Experiments with rotating cylinders for $h/d = 3$.

8. Influence of the wall curvature

The influence of the curvature has been isolated by means of experiments with rotating cylinders. The inner cylinder of diameter D was at rest and the outer cylinder of diameter λD was rotating with a constant frequency N. In order to obtain a large number of values of d/D and d/θ, three outer cylinders and four inner cylinders (two for each value of h/d) were built. The chosen values were $D = 48, 60$ mm and $\lambda D = 64, 72, 84$ mm. The flow between the cylinder was laminar and stable (Schlichting 1979). The velocity was

$$u = \frac{2\pi N \lambda^2}{\lambda^2 - 1}\left(r - \frac{D^2}{4r}\right),$$

r being the distance to the axis. We have

$$u_e^2 \theta = \int_{\frac{1}{2}D}^{\frac{1}{2}\lambda D} (u_e - u)\, u\, \mathrm{d}r$$

d/θ: ▼ 0.07–0.16   ■ 1.12–1.20
            O 0.24–0.28   ▽ 1.5–1.7
            ✿ 0.33–0.41   ▲ 3
            — 0.61   ● 6
            □ 0.75–0.78   ✱ 8–18

$F + G_{\mathrm{c}}\dfrac{d}{D}$ $h/d = 1$

d/θ: ▼ 0.08–0.12   ● 1.1
            ▽ 0.15–0.17   O 1.7–2.2
            ✿ 0.37–0.41   ▲ 3
            ▣ 0.62–0.76   ● 4.6
            — 0.92–0.02   ✱ 8–18

$F + G_{\mathrm{c}}\dfrac{d}{D}$

$h/d = 3$
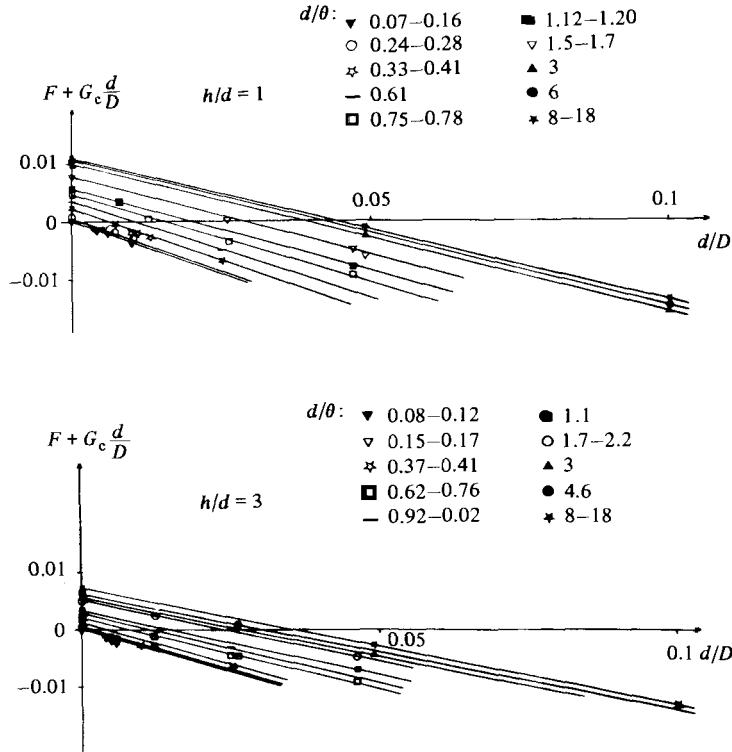
FIGURE 9. Determination of G_{c} in laminar flow.
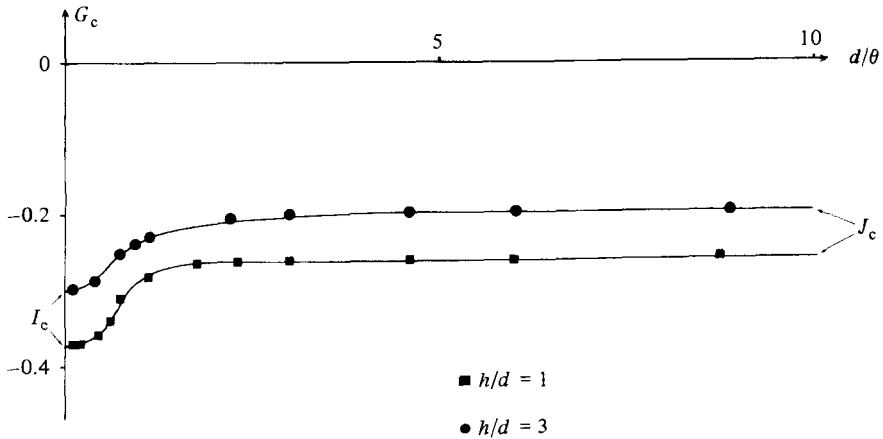
FIGURE 10. Influence of the wall curvature in laminar flow.

with $u_{\mathrm{e}} = \pi D N$, so that

$$\frac{\theta}{D} = \lambda - \frac{2\lambda}{\lambda^2 - 1}\log\lambda - \frac{2\lambda}{(\lambda^2 - 1)^2}\left(\frac{\lambda^4}{3} - 2\lambda^2 + \frac{8\lambda}{3} - 1\right).$$

Here, as λ is smaller than 1.75, θ is very close to $\frac{1}{12}(\lambda - 1)\,D$.

On each inner cylinder an orifice was chosen as a reference (subscript r) and all pressure measurements were made simultaneously between this orifice and the others.

Azimuth	d/mm	$\dfrac{u_{ex}d}{u_e}$	$\dfrac{K_d - K_0}{1 - K_0}$ (measured)	$F_1 + J_v\dfrac{u_{ex}d}{u_e} + J_c\dfrac{d}{D}$ (calculated)
10°	0.34	0.114	0.062	0.063
	0.77	0.258	0.154	0.140
15°	0.34	0.077	0.051	0.046
	0.77	0.173	0.092	0.094
20°	0.34	0.059	0.033	0.036
	0.77	0.135	0.076	0.074
	1.54	0.270	0.125	0.140
25°	0.34	0.049	0.027	0.031
	0.77	0.111	0.060	0.061
	1.54	0.222	0.099	0.100
30°	0.34	0.037	0.020	0.025
	0.77	0.085	0.043	0.047
	1.54	0.170	0.076	0.087
35°	0.34	0.030	0.017	0.020
	0.77	0.068	0.037	0.038
	1.54	0.136	0.063	0.069
40°	0.34	0.024	0.016	0.018
	0.77	0.055	0.029	0.031
	1.54	0.110	0.051	0.055
	3.03	0.215	0.103	0.097
45°	0.34	0.021	0.015	0.016
	0.77	0.046	0.027	0.026
	1.54	0.092	0.045	0.046
	3.03	0.175	0.090	0.080
50°	0.34	0.016	0.013	0.013
	0.77	0.037	0.028	0.022
	1.54	0.074	0.043	0.037
	3.03	0.145	0.080	0.064
55°	0.34	0.011	0.006	0.011
	0.77	0.026	0.013	0.016
	1.54	0.052	0.026	0.024
	3.03	0.103	0.049	0.042
60°	0.34	0.009	0.005	0.009
	0.77	0.021	0.010	0.012
	1.54	0.042	0.022	0.019
	3.03	0.082	0.041	0.031

TABLE 1. Flow around a cylinder with $h/d \approx 3$; verification of (10)

Figure 8 shows some results for $h/d = 3$. The extrapolation gives $p_0 - p_r$: hence, by subtraction, $p_d - p_0$. The dimensionless error is shown on figure 9 versus d/D for various values of d/θ. As more than two points generally correspond to a given d/θ, we can ascertain that the curves we obtain are straight lines. The ordinate at the origin is the laminar value of F as in §7, and the slope is equal to G_c. J_c is obtained by large values of d/θ (in fact for $d > 5\theta$). I_c is obtained in the same manner as I_v; the remark made about the accuracy concerning I_v is also valid for I_c.

The two curves in figure 10 give G_c in terms of d/θ only in laminar flow, except for the extreme values I_c and J_c.

From a practical point of view this result is sufficient because for an airfoil the curvature interferes only in the vicinity of the leading edge where the boundary layer is generally laminar (Ducruet 1983a, b).
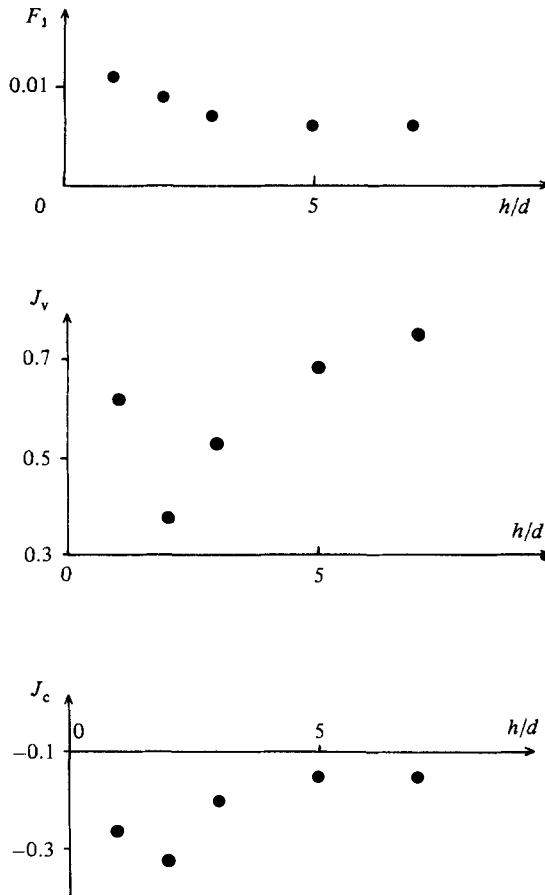
FIGURE 11. Influence of h/d for $d \gg \theta$.

9. Verifications and applications

The method suggested here was applied at first to the flow around a cylinder of diameter $D = 30$ mm in the wind tunnel described in §5. The Reynolds number was close to 5×10^4. Four cylinders were built, each equipped with 4 orifices located on a generatrix. For three of them, h/d is constant and equal to 3, 5 and 7, and d/D lies between 10^{-2} and 10^{-1}. For the fourth cylinder d is constant, and h/d lies between 0.4 and 9.4.

The verification was made for the cylinder with $h/d = 3$. For all cylinders we had $d \gg \theta$, so that (10) had to be used. The results are to be compared to the measured values $(K_d - K_0)/(1 - K_0)$. Of course, the comparison was made upstream of separation. Table 1 shows that results are close to each other when $u_{ex}d/u_e \lesssim 0.15$.

As the method seems satisfactory, we can use the measurements made on the other cylinders to obtain F_1, J_v and J_c for $h/d = 5$ and 7, and also for 2 on the last cylinder, with d/D constant. It appears that F_1 is almost constant for $h/d \geqslant 3$. The same is true concerning J_c for $h/d \geqslant 5$. On the other hand, no asymptotic value of J_v could be reached (figure 11).

Measurements made in the separated domains downstream from the cylinders give results related to (7). This formula seems to be verified (figure 12).
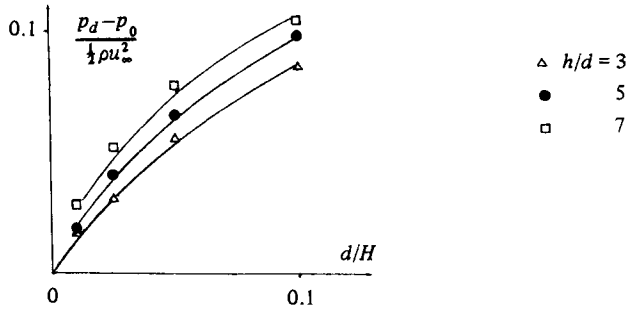
FIGURE 12. The error in a separated domain.

x/l	10^3E $d = 0.3$ mm	10^3E $d = 0.6$ mm	K_0 $d = 0.3$ mm	K_0 $d = 0.6$ mm
0	—	—		
0.0078	74	—	0.683	—
0.0103	51	—	0.450	—
0.0246	23	37	−0.401	−0.400
0.0252	23	37	−0.405	−0.404
0.0338	1	−6	−0.565	−0.562
0.0432	5	2	−0.526	−0.524
0.0460	5	2	−0.444	−0.440
0.0795	7.5	7	−0.339	−0.338
0.0803	8.5	7	−0.336	−0.336
0.1140	8	9	−0.316	−0.314
0.1331	8	9	−0.300	−0.297
0.1609	7.5	9	−0.306	−0.302
0.2796	7	8.5	−0.292	−0.289
0.2800	7	8.5	−0.292	−0.289
0.3797	6.5	8	−0.294	−0.290
0.3813	6.5	8	−0.297	−0.295
0.4796	6	7.5	−0.281	−0.279
0.4816	6	7.5	−0.285	−0.282
0.5800	5.5	7	−0.219	−0.218
0.5818	5.5	7	−0.221	−0.219
0.6807	5.5	7	−0.166	−0.165
0.6820	5.5	7	−0.167	−0.166
0.7813	5.5	7	−0.124	−0.123
0.7827	5.5	7	−0.124	−0.124
0.9493	4.5	6	−0.034	−0.034
0.9500	4.5	6	−0.032	−0.033

TABLE 2. Flow around an ONERA D airfoil; $l = 150$ mm, $u_\infty l/\nu \approx 2.5 \times 10^5$. x is the curvilinear abscissa from the leading edge; E the error calculated with (8).

As for the stagnation point and its vicinity, special measurements were made (Ducruet 1983a). They showed that as $d/D \ll 1$ (6) can be linearized with regard to d/D. In fact the stagnation pressure does not pose problems, because it can easily be calculated with the Bernoulli law.

Our second application concerns an airfoil of chord 150 mm at zero angle of attack and at an upstream velocity $u_\infty \approx 25$ m/s (Ducruet 1983a). Two sets of twenty-seven
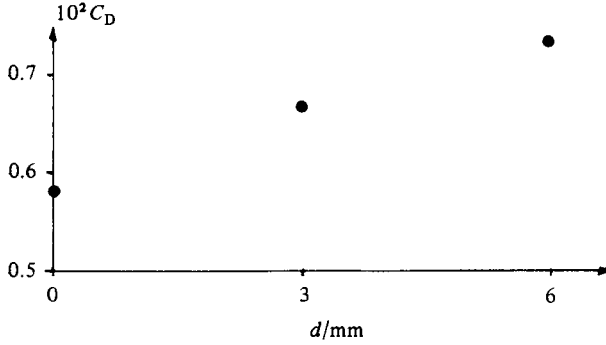
FIGURE 13. Influence on the pressure drag of an airfoil.

orifices of diameter 0.3 mm and 0.6 mm were used. The orifices are located in pairs on the same generatrix, at equal distances from the wind-tunnel walls. In table 2 the two last columns represent the corrected values obtained by applying (8) to the measured pressures for $d = 0.3$ and 0.6 mm. It can be seen that the two orifices lead to almost the same value of K_0.

The actual drag coefficient C_{D0} was calculated by integration of K_0, and then compared with the drag coefficient C_D deduced from the pressures already measured: the result is that C_D is 26 % larger than C_{D0} for $d = 0.6$ mm and 14 % larger for $d = 0.3$ mm (figure 13).

10. Conclusion

As the errors generated by the boundary layer, the velocity gradient and the wall curvature can be of opposite sign, one may look for the value of d that gives $p_d = p_0$. Let us consider similar airfoils of chord l and put $d^* = d/l$, $\theta^* = \theta/l$, $D^* = D/l$, $x^* = x/l$, $u_e^* = u_e/u_\infty$, $\delta = d/\theta$.

Substituting in (8) and equating to zero gives

$$F + \delta\theta^* \left(G_v \frac{u_{ex}^*{}^*}{u_e^*} + \frac{G_c}{D^*} \right) = 0,$$

where u_e^* depends only on x^*, whereas θ^* depends on x^* and $u_\infty l/\nu$.

As F is positive there is a solution if the velocity gradient is negative and (or) if the wall is convex. Of course the obtained value of d must be acceptable: this means it must be positive and such that $u_{ex}d/u_e$ and d/D be small. The difficulty is that the previous value changes with the angle of attack because u_e, u_{ex} and θ change. Consequently, from a practical point of view, the error cannot be avoided.

It must be noticed that the use of the methods of correction is quite difficult. It requires the knowledge of D, u_e, u_{ex} and θ. For two-dimensional flow there is no major difficulty, but that is not the case for three-dimensional flow, especially because the direction of the outer velocity is not known in advance.

All the results presented in §9 show the importance of the method of correction. The need of such a method is particularly evident for cryogenic wind tunnels, where models are small and boundary layers are thin, so that the disturbances generated by the orifices can be important. As cryogenic wind tunnels are built for high-speed flow, the method must be extended to compressible fluid: that remains to be done.

REFERENCES

BARAT, M. 1973 *Techniques de Mesure dans les Ecoulements*, pp. 245–280. Eyrolles.

BENEDICT, R. P. & WYLER, J. S. 1978 Analytical and experimental studies of ASME flow nozzles. *Trans ASME i: J. Fluids Engng* **100**, 265–273.

CHUE, S. H. 1979 *Prog. Aerospace Sci.* **16**, 147–223.

DUCRUET, C. 1983a Détermination exacte de la pression pariétale dans un écoulement. Thesis, University of Lille I.

DUCRUET, C. 1983b Une méthode pour la détermination exacte de la pression pariétale dans un écoulement. *C. R. Acad. Sci. Paris* **296**, II, 309–312.

DUCRUET, C. & DYMENT, A. 1981 Sur la détermination exacte de la pression pariétale dans un écoulement. *C. R. Acad. Sci. Paris* **292**, II, 1349–1351.

EICHELBRENNER, E. R. 1958 La couche limite à trois dimensions. *Publ. Sci. Tech. du Min. de l'Air, Paris*, NT 85, pp. 57–83.

FLACK, R. D. 1978 Static pressur hole errors in transonic flow with pressure gradients. *ISA Trans.* **17**, 89–95.

FRANKLIN, R. E. & WALLACE, J. M. 1970 Absolute measurement of static-hole error using flush transducers. *J. Fluid Mech.* **42**, 33–48.

LIVESEY, J. L., JACKSON, J. D. & SOUTHERN, C. J. 1962 The static hole error problem. *Aircraft Engng* **34**, 43–47.

MORRISSON, D. F., SHEPPARD, L. M. & WILLIAMS, M. J. 1966 Hole size effect on hemisphere pressure distributions. *J. R. Aero. Soc.* **71**, 317–319.

MOULDEN, T. H. *et al.* 1977 Experimental study of static pressure orifice interference. *AEDC* TR 77.57.

MYADZU, A. 1936 Über den Einfluß der Bohrungen auf die Druckanzeige. *Ing. Arch.* **7**, 35–41.

PUGH, P. G., PETO, J. W. & WARD, L. C. 1970 Experimental verification of predicted static hole size effects on a model with large streamwise pressure gradients. *NPL Aero Rep.* 1313, *ARC* 31, 900.

RAINBIRD, W. J. 1967 Errors in measurement of mean static pressure of a moving fluid due to pressure holes. *DME/NAE Q. Bull.* 1967 (3), pp. 55–89.

RAY, A. K. 1956 On the effect of orifice size on static pressure reading at different Reynolds numbers. *Transl. in ARC Rep.* TP 498.

RAYLE, R. E. 1949 An investigation of the influence of orifice geometry on static pressure measurement. MS thesis, MIT.

SCHLICHTING, H. 1979 *Boundary Layer Theory*. McGraw-Hill.

SHAW, R. 1960 The influence of hole dimensions on static pressure measurements. *J. Fluid Mech.* **7**, 550–563.

ZOGG, H. & THOMANN, H. 1972 Errors in static pressure measurements due to protruding pressure taps. *J. Fluid Mech.* **54**, 489–494.